High-throughput computational analysis of kinetic barriers to ring-closing depolymerization for aliphatic polycarbonates

Brandi Ransom,[1,*] Riccardo Bosio,[1,†] Dmitry Zubarev,[1] James L. Hedrick[1], and Nathaniel H. Park[1,*]

[1]IBM Research–Almaden, 650 Harry Rd. San Jose, CA 95120

†Present address: École Polytechnique Fédérale de Lausanne, Rte Cantonale, 1015 Lausanne, Switzerland

*Corresponding author. Email: Brandi.Ransom@ibm.com

Abstract

The chemical reversion of polymers via ring-closing depolymerization (RCD) to their monomeric constituents is a highly promising avenue to enable end of life-cycle recycling and reuse. However, most reported systems using RCD revolve around bespoke monomer designs to facilitate facile depolymerization and there exists relatively few investigations into influence of functional groups on the ability of a particular monomer to cleanly undergo depolymerization. Here, we perform computational investigations into the energy barriers for RCD of 6-membered aliphatic carbonates in different solvents. The results demonstrate highlight clear trends observed in prior experimental studies, validating the utility of computational investigations towards understanding RCD. Experimental evaluation of thermal depolymerization of two monomers confirmed the ability of the computationally investigated monomers to cleanly undergo RCD. Overall, this work highlights the utility of high-throughput energy barrier computations to provide meaningful insight into broad reactivity trends that would be highly laborious to access experimentally.

Introduction

Polymeric materials are ubiquitous in the modern economy due to their broad range of properties and mass production from commodity feedstocks. However, this utility came at the cost of severe environmental contamination from waste plastics and their byproducts from mechanical (microplastic formation) or chemical degradation. Current solutions typically favor mechanical recycling, which inherently lowers the quality of any products, low-oxygen pyrolysis, which is more energy intensive, returns plastics to crude oil, naptha, or fuel, but is more energy intensive and produces toxic byproducts such as dioxin from halogenated polymers.[1–3] In contrast, chemical recycling through depolymerization has the potential to be more tolerant of contamination and mixed-waste streams—avoiding the laborious pre-sorting required for other recycling techniques.[4,5] In contrast to mechanical recycling, chemical recycling to monomers may allow for regeneration of the respective parent material of the same quality.[6–8] However, despite significant efforts, many processes face severe technical and economic hurdles—ranging from materials and catalyst design to reaction optimization on mixed waste streams—and hence are only utilized on less than 5% of plastic waste.[6]

Given these extensive experimental challenges in chemical recycling, the development of assistive computational and informatics toolkits will undoubtedly accelerate efforts to develop

scalable chemical recycling technology. Ring-closing depolymerization (RCD) is process which the ceiling temperature (T_c) of a polymeric material is exceeded to favor selective reversion to monomer under thermal or catalytic conditions (Fig. 1A and Fig. 1B).[7–9] Many systems which utilize RCD have focused on designing custom monomers with unique structural features to influence ΔH_p and ΔS_p, and hence the T_c.[10–13] Specifically, these features often include geminal di-substitution, incorporation of bridged or fused ring systems, and increasing transannular strain.[10–14] In addition to monomer design, careful selection of an appropriate catalyst, solvent, and other reaction parameters can lower the T_c and favor depolymerization.[15] Despite these advances, it remains challenging broadly to assess potential depolymerization ability across numerous polymer classes solely based on monomer structural features—hampering the efforts to use RCD in systems where highly optimized monomer structures have already been developed. While computational and machine-learning models have been developed for predicting the ΔH_p for ring-opening polymerization (ROP) which can help inform the propensity for RCD,[16,17] we sought to develop a more holistic approach to better understand the complex interrelationships between monomer structural features and reaction parameters in RCD. Here, we developed a computational framework to aid in understanding the effects of solvent–monomer interactions on the kinetic barriers to depolymerization as applied to a variety of aliphatic 6-membered cyclic carbonates.

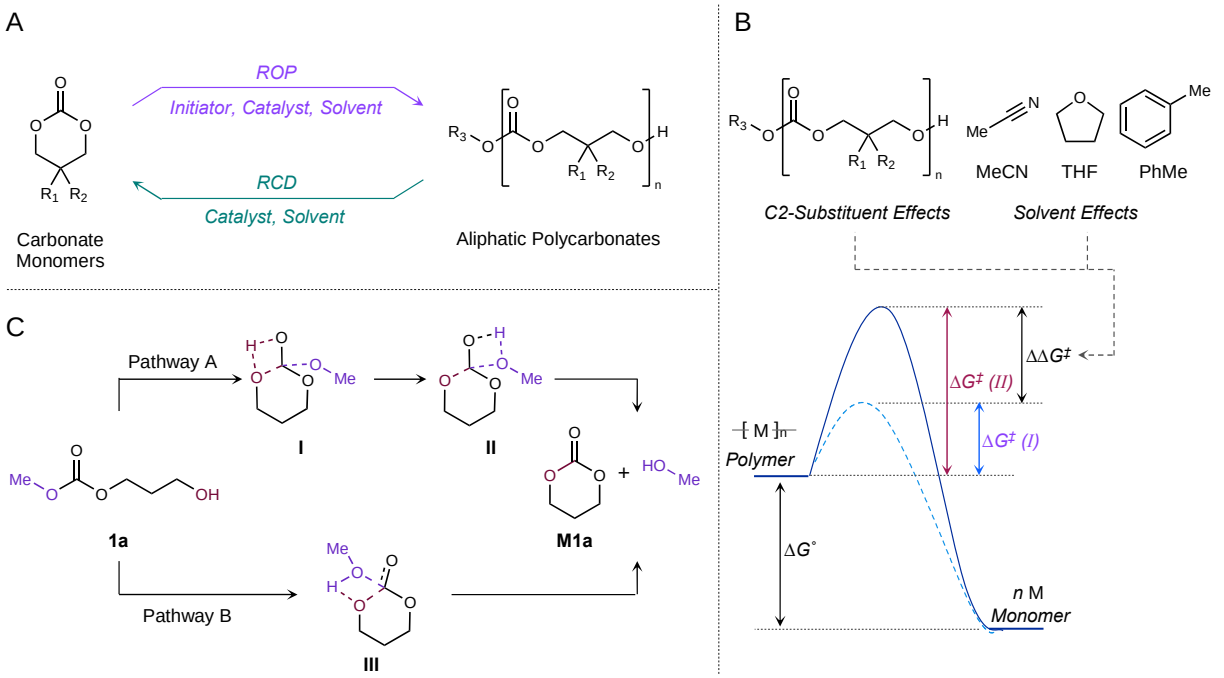

Figure 1. A) Depiction of ring-opening polymerization (ROP) and ring-closing depolymerization (RCD) of polycarbonate systems. B) Depiction of the potential influence of substituent effects and solvent effects on RCD barrier height. C) Two potential pathways for RCD modeled in the computational methodology.

Given the ease of accessibility of highly functionalized 6-membered carbonates from abundant feedstocks and their broad range of applications, understanding the propensity of these systems to undergo controlled RCD will provide needed insight into fundamental reactivity trends. In contrast to cyclic lactones,[9,11] there is significantly less known on the structural influences in 6-membered carbonates over their thermodynamic polymerization parameters (ΔH_p, ΔS_p), making it difficult to ascertain *a priori* the effect of functional group modifications on the T_c, let alone the depolymerization reaction kinetics. Indeed, there are only a handful of reports investigating depolymerization of 6-membered aliphatic polycarbonates[15,18–23] or other ring-sizes in general.[7,14]

Although addition of geminal di-substitution or fused/bridged/spiro rings are effective for lactones and lactams to improve depolymerizability,[10–13] these impact of these features in 6-membered cyclic carbonates on the polymerization process, the ΔH_p and ΔS_p of the monomer, and the kinetics of depolymerization under different conditions are poorly understood. Finally, while ΔH_p and ΔS_p are useful in assessing the thermodynamic potential for depolymerization, it is experimentally unfeasible to measure them across all monomer types and reaction conditions and moreover, these values do not provide information on the energy barrier to RCD (Fig. 1C). Thus, there exists a need for computational methodology to provide insight into complex reactivity trends in regimes where accessing experimental data is costly and historical data is minimal. Here, we show that using empirical computational techniques such as Density-Functional Tight-Binding (DFTB), it is possible to more quickly explore monomer chemical space and build understanding around potential solvent–structure interrelationships via analysis of enthalpic barriers to depolymerization. In turn, this high-throughput barrier characterization process can be used for screening of depolymerization of polycarbonate oligomers and act as an upper bound on quantitative measurements.

Methods

Reaction Coordinate Definition and Monomer Standardization

We utilized Potential Energy Scans with the AMS Software with the CHON-2019 Reax ForceField to estimate transition barriers from the linear carbonates to its corresponding cyclic carbonate and methanol via two paths based on hydrogen atom position (Fig. 1C). RDkit was used to standardize the starting point of each linear carbonate system by recreating the geometries of different functional groups attached to the C2-carbon (Fig. 1B) in the carbonate monomer. This code only requires the SMILES representation of the functional group which will be attached. The structures of all the corresponding cyclic carbonate monomers investigated are provided in Fig. 2A (**1a**–**g**) and Supplementary Fig. 1 (**2a–ar**).

Conformational Analysis

The standardized carbonates only received the minimum MMFF for relaxation. In order to ensure we are comparing minimum transition barriers between molecules, we identified the lowest energy monomer for each state along the reaction coordinate. With RDKit, 100 conformers are generated for each carbonate and state, which are then undergo geometry optimization with DFTB. For the transition state (TS) conformers, the transferred hydrogen atom, bonded oxygen atoms, and tetrahedral carbon are constrained during the relaxation, to preserve each of the three specific transition states undergoing optimization. For our benchmarked materials, the 10 conformers which showed the most structural diversity—as measured by RDKit—and are within the lowest 5 kcal/mol energetically, were then optimized at the B3LYP level to find the lowest energy conformation.

Molecular and Quantum Methods

To screen large numbers of compounds for qualitative exploration of linear carbonate functional space, we utilized accessible levels of theory that can perform optimization calculations on a reasonable time scale. *Ab initio* calculations with B3LYP orbitals are not tractable on a large scale, however we compute *ab initio* energies for three monomers to show the qualitative comparison between other levels of theory. To compare energetics in isolation, each of the states were

optimized at the B3LYP level in gas phase after being optimized with DFTB for TS optimizations and geometry optimizations. The chosen representative conformers were then calculated with single point DFTB for the energetics discussed in the results section. Gaussian software was used for *ab initio* geometry relaxations and transition state optimizations with a convergence criteria of 10^{-6} *Hartree/bohr*.[24] Amsterdam modeling suite was used to carry out DFTB calculations, with PM7 and GFT1-N parametrizations, respectfully.[25,26] Solvents were added to DFTB through a continuum model with 230 points to create the mesh for interactions, an implementation of the generalized born and surface area model.[27] By utilizing this scheme with multiple levels of theory, we can explore a much wider materials space. DFTB calculations take less than one minute for an optimization, and optimizations with Gaussian can take several hours, even for our molecules which all have less than 40 atoms. We estimate an increase in speed of approximately 2 or 3 orders of magnitude.

Molecule Space Investigations

To survey the molecular space of potential carbonate for steric and electronic features which may correlate with lower depolymerization barrier height, we first selected seven core carbonate monomers (**1a**-**g**, Fig. 2A) which exhibit systematically varied steric and electronic effects while still being computationally approachable for DFT optimizations. To expand this dataset for exploration using the more efficient DFTB methodology, we first mined 196 cyclic carbonate monomers with pendant chains contain 30 atoms or less from patent literature using IBM's Chemical Information Resources for Cognitive Analytics (CIRCA) platform as well as from historical experimental data.[28] We next computed both the depolymerization barrier height and 1613 Mordred features for corresponding linear carbonates of **1a**-**g** (Fig. 2A).[29] Using the top 20 most positively and negatively correlated features, we calculated the distribution of the features for all CIRCA-found molecules and reduced the feature set by removing features with similar distributions as determined with a Kolmogorov-Smirnov test and a p-value < 0.05. For each of the remaining 27 Mordred features, we divided the range of possible feature values into 10 bins and select one molecule to represent each bin range, provided it is not already represented by **1a**-**g** (Fig. 1). Following this procedure, we identified 26 additional molecules which were used in the DFTB barrier protocol to examine property–barrier trends.

Results

Four specific states were chosen to best represent the initial, TS, and final states of the depolymerization reaction with the knowledge that these could not be comprehensive to all the bond rotations and extensions. The exact, optimized configurational response along the polymer chain during the TS cannot be accurately captured as it is a specific energetic path in the potential landscape. As electron withdrawing effects of pendent functional groups drop off significantly along the polymer backbone, we only examine a single repeat unit for comparison of qualitative energetics between *ab initio* and semi-empirical methods. Additionally, using longer chains would need to be frozen in *ab initio* calculations to make them tractable while in semi-empirics they would be extremely susceptible to fall into local minima. Keeping a longer polymer chain would also necessitate freezing atoms, and we would only be able to compare the solvent effects for larger materials with a higher degree of polymerization (DP_n).

A

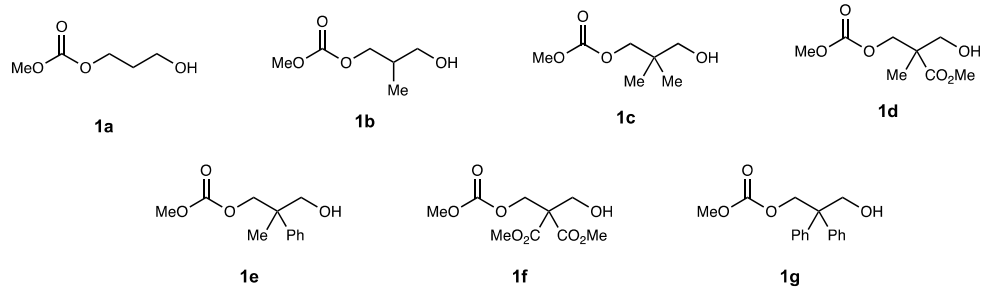

B

Compound	Barrier MeCN (kcal/mol)	Barrier PhMe (kcal/mol)	Barrier THF (kcal/mol)	Volume (Å^3)
1a	45.96.	44.15	43.96	77.14
1b	43.55	44.26	44.20	89.70
1c	45.35	48.14	47.65	102.3
1d	43.87	45.83	47.78	131.1
1e	45.56	45.09	47.33	152.3
1f	43.61	45.62	47.01	159.2
1g	43.82	44.11	44.43	202.5

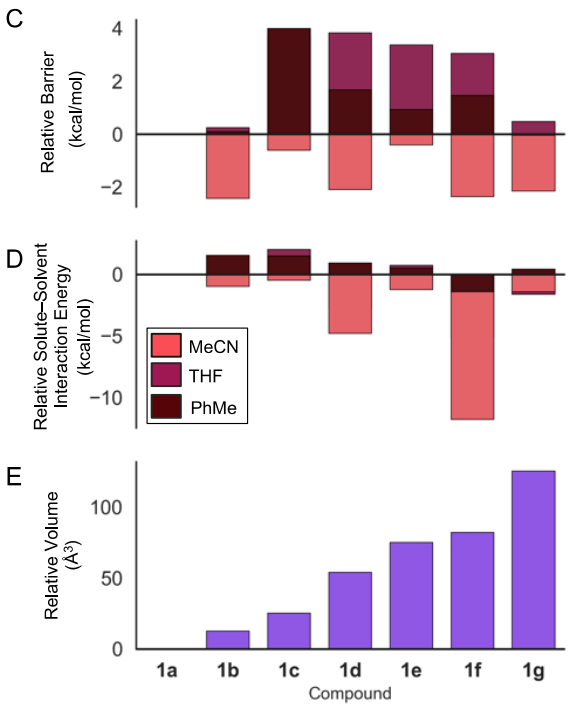

Figure 2. Plot of barrier height, solvent interaction, and volume relative to trimethylene carbonate (**1a**) for the **1a-1g.** Barrier height and solvent interaction include values for three different solvents: toluene (PhMe), acetonitrile (MeCN), and tetrahydrofuran (THF). See Supporting Information for full bar plot of all relative values and absolute values of the energy barriers.

The results of the DFT optimized barriers from **1a**–**g** (Fig. 2A) are shown Fig. 3, with the average absolute enthalpic energy barriers ranging around 40 kcal/mol (Fig. 2B) for an uncatalyzed ring closure to re-form a cyclic carbonate (Fig. 1B). From the absolute enthalpic barriers alone it is challenging to ascertain a clear trend in terms of the computed volume or solvent interaction energy. Instead, by plotting the difference in the energy barrier or solvent interaction energy for each compound relative to **1a**—which bears only hydrogen atoms attached to its C2 carbon—we can observe changes in the energy barrier which may correspond to the steric and electronic effects of the substituents at the C2 carbon in conjunction with respective solvent environment (Fig. 2C and Fig 2D). From these plots, it is apparent that using acetonitrile (MeCN) as a solvent universally lowers the relative enthalpic barrier to depolymerization by over 2 kcal/mol in some instances (Fig 2C). In contrast, use of toluene (PhMe) or tetrohydrofuran (THF) as solvents lead to an increase of the relative energy up to nearly 4 kcal/mol. Similar trends are also observed in the DFT

computed enthalpic barriers where MeCN typically gave the lower enthalpic barrier heights, albeit that the DFT computed barriers are approximately 1-5 kcal/mol higher relative to the corresponding DFTB computed ones (Fig. 3). Analogous trends are seen also with the solvent interaction energy, where again use of MeCN universally lead to lower values (Fig. 2D). With the computed volume relative to **1a** (Fig. 2D), no apparent correlation was observed with changes in relative solvent interaction energy or relative enthalpic barrier height across all solvents.

A

Compound	Barrier MeCN (kcal/mol)		Barrier PhMe (kcal/mol)		Barrier THF (kcal/mol)	
	DFT	DFTB	DFT	DFTB	DFT	DFTB
1a	51.67	45.96	52.24	44.15	51.84	43.96
1b	51.05	43.55	50.92	44.26	50.83	44.20
1c	54.44	45.36	55.21	48.15	56.03	47.65
1d	49.86	43.87	54.85	45.83	47.11	47.79
1e	46.53	43.61	53.20	45.62	47.57	47.02
1f	53.39	45.56	55.89	45.09	54.93	47.33
1g	51.48	43.82	51.27	44.11	51.35	44.44

B

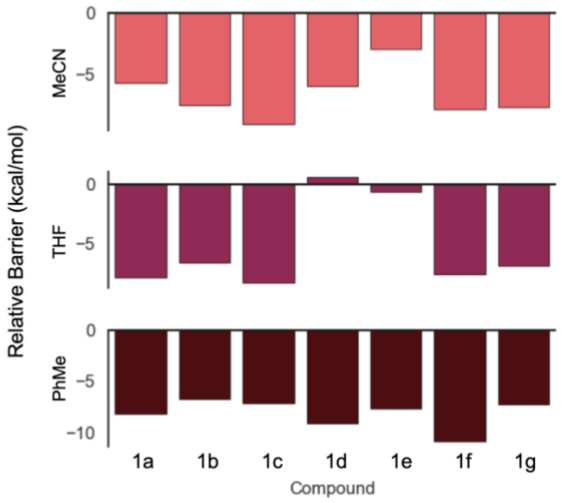

Figure 3. Comparison of DFT and DFTB barrier heights for **1a-1g**. A) Table of absolute DFT and DFTB energy barriers for MeCN, PhMe, and THF. B) Relative difference between DFTB and DFT energy barriers in MeCN, THF, and PhMe.

Prior experimental work had observed trends in the depolymerization of many of the same or similar monomers under thermodynamic control, where sterically bulkier substituents at the C2-carbon in general favored higher yields of the corresponding cyclic carbonate (see Supplementary Fig. 2 for summarized literature examples).[19] Based on the computational enthalpic barrier data presented here, the correlation between the steric size of the C2-substituents and either the absolute or relative enthalpic barriers is less clear when MeCN is used as solvent whereas PhMe and THF do show in general decreasing barrier heights from **1c** to **1g** as the molecular volume increases (Fig. 2B and D). This is roughly consistent with prior thermodynamic trends observed when using THF and suggests when using these solvents bulkier substituents give both a faster rate and stronger thermodynamic driving force.[19] While the overall interrelationships between solvent, structural features, and enthalpic barrier are complex, the overall trends with the solvent interaction energies, enthalpic barrier height, and solvent identity are more clear and correlate well with experimental observations on the solvent effect on the T_c. In reported experimental work, non-polar solvents such PhMe resulted in higher T_c values compared to polar aprotic solvents such as MeCN.[15] This trend is also generally observed in the DFTB absolute and relative enthalpic barriers where MeCN is utilized, suggesting that MeCN not only lowers the T_c, but also accelerate the reaction as well. From published experimental results, polar aprotic solvents also tend to give better results in terms of conversion to monomer whereas nonpolar solvents give poorer results (Supplementary Fig. 2).[15,18–22] As the thermodynamic interpretation of the reported solvent-solute interaction is the contribution to the free energy from vacuum to solvated, a negative contribution from MeCN suggests the molecules are able to achieve tighter conformations. MeCN is allowing

conformations which would typically require a higher temperature to access, likely by screening intramolecular interactions.

The overall enthalpic barriers for **1a-g** to RCD are high, which is anticipated for an uncatalyzed transformation. In a previously reported kinetic study, the DBU catalyzed RCD of an aliphatic polycarbonate (based on the monomer **S1c**, Supplementary Fig. 2) in MeCN was observed to have a k_{app} = 6.4 x 10^{-4} s^{-1} corresponding approximately to a $\Delta G^{\ddagger}$ of 26.1 kcal/mol.[15] This value is roughly half of the enthalpic barriers computed for **1a-g** via DFT or DFTB in MeCN, which of course may still vary significantly in total energy depending on the entropic contributions. The stark difference between these values highlights the critical role of catalysts in facilitating the RCD transformation in solution as well as the kinetic trapping of these systems in the polymeric state.[8,9] Nonetheless, as noted above, useful trends can be observed in the relative changes of the enthalpic barrier as a function of different conditions. Given the height of the enthalpic barrier, we opted to verify experimentally the uncatalyzed thermal depolymerization of the corresponding polymers of **1c** and **1d** under neat conditions. Here, the RCD at 230 °C for 12 h gave **M1c** and **M1d** in approximately 67% and 63% conversion, respectively, as determined by relative ratios of their NMR peaks (Supplementary Fig. 3).

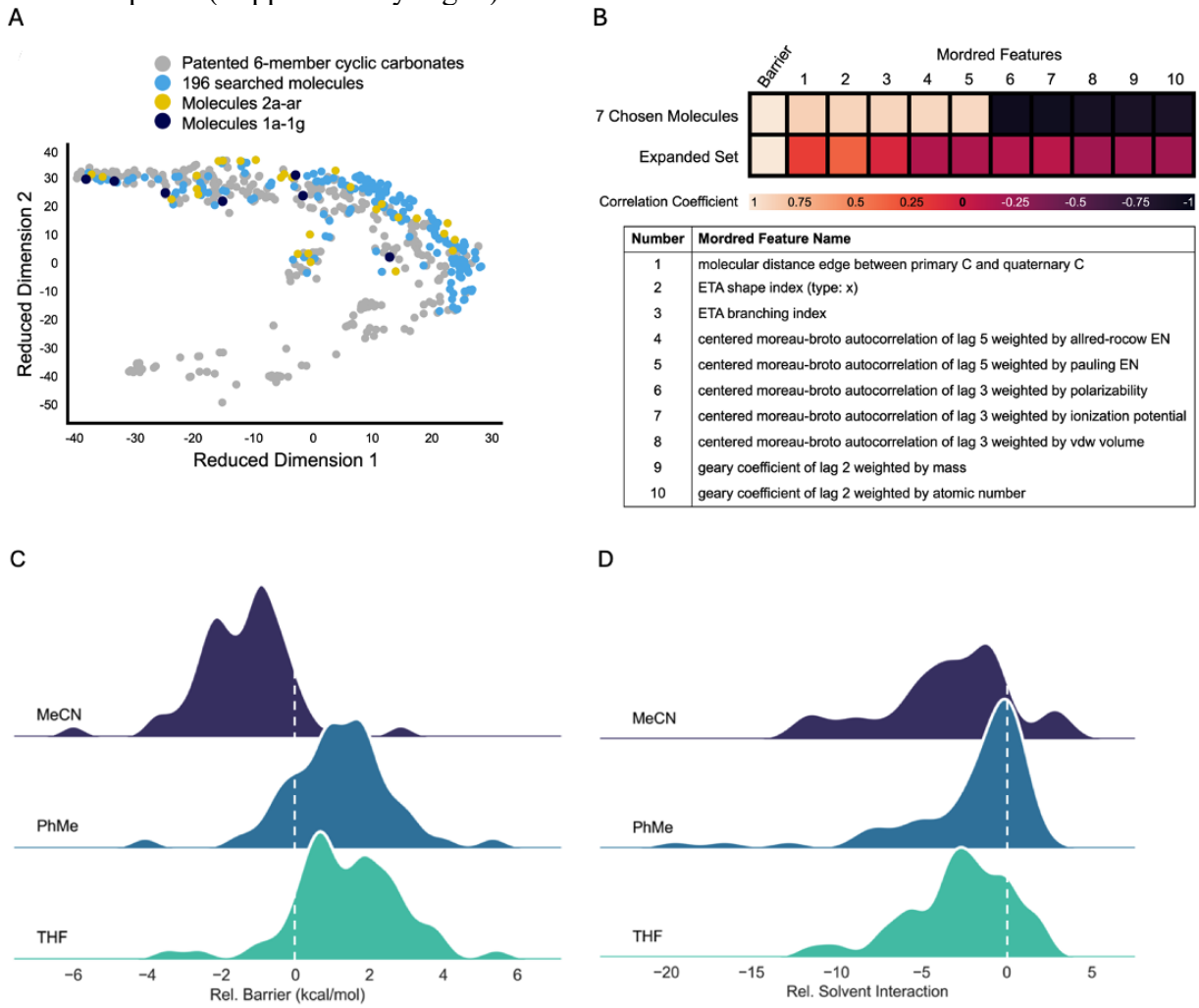

Number	Mordred Feature Name
1	molecular distance edge between primary C and quaternary C
2	ETA shape index (type: x)
3	ETA branching index
4	centered moreau-broto autocorrelation of lag 5 weighted by allred-rocow EN
5	centered moreau-broto autocorrelation of lag 5 weighted by pauling EN
6	centered moreau-broto autocorrelation of lag 3 weighted by polarizability
7	centered moreau-broto autocorrelation of lag 3 weighted by ionization potential
8	centered moreau-broto autocorrelation of lag 3 weighted by vdw volume
9	geary coefficient of lag 2 weighted by mass
10	geary coefficient of lag 2 weighted by atomic number

Figure 4. A) TSNE plots of the DFT computed set (**1a-g**) and the DFTB set (**2a-ar**). B) Comparison of the correlation of Mordred features of **1a-g** and **2a-ar** DFTB-computed energy barriers to RCD. C) Kernel density plot of distribution of the depolymerization barriers relative to **1a** for all carbonates. D) Kernel density plot for distribution of the solvent interactions relative to **1a** for. White dashed line in both plots indicates zero or no change in solvent interaction or energy barrier relative to **1a**.

Having evaluated the trends of the enthalpic barriers for carbonates **1a-g**, we next sought to determine whether these would prove generalizable to a much broader set of potential aliphatic carbonate systems with very different types of functional groups. As noted in the Methods section, the selection protocol used for identifying **2a-ar** (Supplementary Fig. 1) specifically targeted molecules containing Mordred features not present in the **1a-g**. However, this method did not evenly cover all groups of molecules within the search space, based on the low-dimensional representation (Fig. 4A). Comparison the correlation of Mordred features to the DFTB-computed energy barrier shows a dramatic variation between features shared by the two datasets (Fig. 4B). Additionally, the most strongly correlated feature from **2a-ar** is the *number of hydrogen bond donors* (0.47), which is much lower than the most strongly correlated features from **1a-g** (Fig. 4B). Additionally, while some of the monomers from the expanded **2a-ar** dataset contain examples of systems that have potentially reactive pendant functional groups (for example, **2d** and **2e**, Supplementary Fig. 1) that may interfere with RCD under experimental evaluation, it is still illustrative to include them as part of examining broader trends across a diversity of carbonate systems.

As with carbonates **1a-g**, we examined the distribution of relative differences in RCD energy barriers and solvent interaction energy for **2a-ar** as compared to **1a** (Fig. 4C and 4D). Consistent with what is observed for **1a-g**, enthalpic barriers computed using MeCN resulted in nearly all carbonate systems having lower barriers for RCD relative to **1a**, with several systems having energy barriers drop by up to 6 kcal/mol (Fig. 4C). The relative solvent interaction energy in general showed mostly negative values relative to **1a** for all solvents, with PhMe seemingly having more values clustered near 0 relative to **1a** (Fig. 4D). This is in line with what is observed for **1a-g** where monomers have non-aliphatic side chains having stronger interactions with solvent (Fig. 2D) considering most of the carbonates **2a-ar** have non-aliphatic side chains and tend to have stronger solvent interactions (Fig. 4D, Supplementary Fig. 1). As with **1a-g** there does not appear to be a direct correlation between enthalpic barrier height, solvent interaction energy, and molecular volume.

Conclusion

Understanding how structure and reaction conditions influence both thermodynamic and kinetic factors affecting RCD of polycarbonates is critical to make informed decisions about the design and application of fully recyclable systems. Experimental kinetic evaluation of broad classes of polycarbonate systems containing a variety of pendant functional groups is highly tedious and labor intensive—hence reported systems for RCD of both polyesters and polycarbonates contain few examples, a narrow compositional design space, and few if any kinetic investigations of RCD.[10–13,15,18–22] Consequently, we have demonstrated the utility of using DFTB methodology for accurate quantification of enthalpic barriers to RCD which is computationally feasible to perform on larger, more diverse datasets. Additionally, this approach allows simplification of the computation to single repeat unit, both avoiding the pitfalls of trying to model a full polymer chain while still capturing the overall trends on the influence of solvent on the enthalpic RCD barrier—which track well with reported influences of solvents on thermodynamic parameters such as T_c.[15]

References

1. Osterath, B. Cracken oder Einschmelzen. *Nachrichten Aus Chem.* **68**, 22–25 (2020).
2. Schyns, Z. O. G. & Shaver, M. P. Mechanical Recycling of Packaging Plastics: A Review. *Macromol. Rapid Commun.* **42**, 200015 (2021).
3. Billiet, S. & Trenor, S. R. 100th Anniversary of Macromolecular Science Viewpoint: Needs for Plastics Packaging Circularity. *ACS Macro Lett.* **9**, 1376–1390 (2020).
4. Spicer, A. J., Brandolese, A. & Dove, A. P. Selective and Sequential Catalytic Chemical Depolymerization and Upcycling of Mixed Plastics. *ACS Macro Lett.* **13**, 189–194 (2024).
5. Arifuzzaman, M. *et al.* Selective deconstruction of mixed plastics by a tailored organocatalyst. *Mater. Horiz.* **10**, 3360–3368 (2023).
6. Jehanno, C. *et al.* Critical advances and future opportunities in upcycling commodity polymers. *Nature* **603**, 803–814 (2022).
7. Coates, G. W. & Getzler, Y. D. Y. L. Chemical recycling to monomer for an ideal, circular polymer economy. *Nat. Rev. Mater.* **5**, 501–516 (2020).
8. Shi, C. *et al.* Design principles for intrinsically circular polymers with tunable properties. *Chem* **7**, 2896–2912 (2021).
9. Olsén, P., Odelius, K. & Albertsson, A.-C. Thermodynamic Presynthetic Considerations for Ring-Opening Polymerization. *Biomacromolecules* **17**, 699–709 (2016).
10. Tian, J.-J. *et al.* Redesigned Nylon 6 Variants with Enhanced Recyclability, Ductility, and Transparency. *Angew. Chem. Int. Ed.* **63**, e202320214 (2024).
11. Tu, Y.-M., Gong, F.-L., Wu, Y.-C., Cai, Z. & Zhu, J.-B. Insights into substitution strategy towards thermodynamic and property regulation of chemically recyclable polymers. *Nat. Commun.* **14**, 3198 (2023).

12. Zhou, L. *et al.* Chemically circular, mechanically tough, and melt-processable polyhydroxyalkanoates. *Science* **380**, 64–69 (2023).
13. Li, X.-L., Clarke, R. W., Jiang, J.-Y., Xu, T.-Q. & Chen, E. Y.-X. A circular polyester platform based on simple gem-disubstituted valerolactones. *Nat. Chem.* **15**, 278–285 (2023).
14. Zhang, W. *et al.* Highly Reactive Cyclic Carbonates with a Fused Ring toward Functionalizable and Recyclable Polycarbonates. *ACS Macro Lett.* **11**, 173–178 (2022).
15. Olsén, P., Undin, J., Odelius, K., Keul, H. & Albertsson, A.-C. Switching from Controlled Ring-Opening Polymerization (cROP) to Controlled Ring-Closing Depolymerization (cRCDP) by Adjusting the Reaction Parameters That Determine the Ceiling Temperature. *Biomacromolecules* **17**, 3995–4002 (2016).
16. Toland, A. *et al.* Accelerated Scheme to Predict Ring-Opening Polymerization Enthalpy: Simulation-Experimental Data Fusion and Multitask Machine Learning. *J. Phys. Chem. A* **127**, 10709–10716 (2023).
17. Tran, H. *et al.* Toward Recyclable Polymers: Ring-Opening Polymerization Enthalpy from First-Principles. *J. Phys. Chem. Lett.* **13**, 4778–4785 (2022).
18. Miyagawa, T., Shimizu, M., Sanda, F. & Endo, T. Six-Membered Cyclic Carbonate Having Styrene Moiety as a Chemically Recyclable Monomer. Construction of Novel Cross-Linking−De-Cross-Linking System of Network Polymers. *Macromolecules* **38**, 7944–7949 (2005).
19. Matsuo, J., Aoki, K., Sanda, F. & Endo, T. Substituent Effect on the Anionic Equilibrium Polymerization of Six-Membered Cyclic Carbonates. *Macromolecules* **31**, 4432–4438 (1998).

20. Endo, T., Kakimoto, K., Ochiai, B. & Nagai, D. Synthesis and Chemical Recycling of a Polycarbonate Obtained by Anionic Ring-Opening Polymerization of a Bifunctional Cyclic Carbonate. *Macromolecules* **38**, 8177–8182 (2005).

21. Endo, T. & Nagai, D. A Novel Construction of Ring-Opening Polymerization and Chemical Recycling System. *Macromol. Symp.* **226**, 79–86 (2005).

22. Darensbourg, D. J., Moncada, A. I. & Wei, S.-H. Aliphatic Polycarbonates Produced from the Coupling of Carbon Dioxide and Oxetanes and Their Depolymerization via Cyclic Carbonate Formation. *Macromolecules* **44**, 2568–2576 (2011).

23. Olsén, P., Odelius, K. & Albertsson, A.-C. Ring-Closing Depolymerization: A Powerful Tool for Synthesizing the Allyloxy-Functionalized Six-Membered Aliphatic Carbonate Monomer 2-Allyloxymethyl-2-ethyltrimethylene Carbonate. *Macromolecules* **47**, 6189–6195 (2014).

24. Frisch, M. J. *et al.* Gaussian 16 Rev. C.01. (2016).

25. R. Rüger, A. Yakovlev, P. Philipsen, S. Borini, P. Melix, A.F. Oliveira, M. Franchini, T. van Vuren, T. Soini, M. de Reus, M. Ghorbani Asl, T. Q. Teodoro, D. McCormack, S. Patchkovskii, T. Heine, AMS DFTB 2022.1, SCM, Theoretical Chemistry, Vrije Universiteit, Amsterdam, The Netherlands, http://www.scm.com.

26. Grimme, S., Bannwarth, C. & Shushkov, P. A Robust and Accurate Tight-Binding Quantum Chemical Method for Structures, Vibrational Frequencies, and Noncovalent Interactions of Large Molecular Systems Parametrized for All spd-Block Elements (Z = 1–86). *J. Chem. Theory Comput.* **13**, 1989–2009 (2017).

27. Ehlert, S., Stahn, M., Spicher, S., Grimme, S. Robust and Efficient Implicit Solvation Model for Fast Semiempirical Methods. *J. Chem. Theory Comput.* **17**, 7 (2021).

28. IBM CIRCA. https://circa.res.ibm.com/.

29. Moriwaki, H., Tian, Y.-S., Kawashita, N. & Takagi, T. Mordred: a molecular descriptor calculator. *J. Cheminformatics* **10**, 4 (2018).